Direct imaging of thermally-activated grain-boundary diffusion in Cu/Co/IrMn/Pt exchange-bias structures using atom-probe tomography

Florent Letellier, Luc Lechevallier, Rodrigue Lardé, Jean Marie Le Breton, K. Akmaldinov, S. Auffret, B. Dieny, Vincent Baltz

Direct imaging of thermally-activated grain-boundary diffusion in Cu/Co/IrMn/Pt exchange-bias structures using atom-probe tomography

F. Letellier,[1] L. Lechevallier,[1,2] R. Lardé,[1] J.-M. Le Breton,[1,a)] K. Akmaldinov,[3,4] S. Auffret,[3] B. Dieny,[3] and V. Baltz[3,b)]
[1]*Groupe de Physique des Matériaux, UMR 6634 CNRS/Université et INSA de Rouen, F-76801 Saint Etienne du Rouvray, France*
[2]*Département de GEII, Université de Cergy-Pontoise, F-95031 Cergy-Pontoise, France*
[3]*SPINTEC, Univ. Grenoble-Alpes/CNRS/INAC-CEA, F-38000 Grenoble, France*
[4]*CROCUS Technology, F-38025 Grenoble, France*

(Received 12 June 2014; accepted 18 November 2014; published online 26 November 2014)

Magnetic devices are often subject to thermal processing steps, such as field cooling to set exchange bias and annealing to crystallize amorphous magnetic electrodes. These processing steps may result in interdiffusion and the subsequent deterioration of magnetic properties. In this study, we investigated thermally-activated diffusion in Cu/Co/IrMn/Pt exchange biased polycrystalline thin-film structures using atom probe tomography. Images taken after annealing at 400 °C for 60 min revealed Mn diffusion into Co grains at the Co/IrMn interface and along Pt grain boundaries for the IrMn/Pt stack, i.e., a Harrison type C regime. Annealing at 500 °C showed further Mn diffusion into Co grains. At the IrMn/Pt interface, annealing at 500 °C led to a type B behavior since Mn diffusion was detected both along Pt grain boundaries and also into Pt grains. The deterioration of the films' exchange bias properties upon annealing was correlated to the observed diffusion. In particular, the topmost Pt capping layer thickness turned out to be crucial since a faster deterioration of the exchange bias properties for thicker caps was observed. This is consistent with the idea that Pt acts as a getter for Mn, drawing Mn out of the IrMn layer. © *2014 AIP Publishing LLC*.
[http://dx.doi.org/10.1063/1.4902954]

I. INTRODUCTION

The field of spintronics uses magnetic multilayers for a number of applications.[1] The multilayers often employ ferromagnetic (F)/antiferromagnetic (AF) exchange biased (EB) bilayers[2,3] and F/insulator (I) bilayers for tunnel magnetoresitance (TMR) in magnetic tunnel junctions (MTJs).[4] Various thermal treatments are required to functionalize these magnetic multilayers. Annealing at a range of 200–500 °C and subsequent cooling in the presence of a magnetic field are essential to crystallize the tunnel barrier and set the exchange bias direction, respectively. These thermal processing steps may result in interdiffusion at the atomic scale[5,6] and deteriorate the magnetic properties.

A great deal of work relates Mn diffusion to annealing temperatures in typical magnetic tunnel junctions.[7,8] It is well-established that Mn atoms diffuse toward the tunnel barrier (AlO_x or MgO) in exchange-biased MTJs. The presence of Mn impurities in or around the tunnel barrier can greatly reduce the TMR. In prior work, oxygen-assisted diffusion was proposed as the most likely mechanism for Mn in exchange-biased MTJs.[8,9] In the present work, we present a study of Mn diffusion activated by the exchange biased couple alone, without the presence of oxide tunnel barriers, excluding oxidation-enhancement of Mn diffusion. In this context, the precise localization of the atoms at the sub-nanoscale and the subsequent deep understanding of the physics of thermally activated interdiffusion in magnetic multilayers is crucial. Many techniques are available for chemical analysis, like high-resolution transmission electron microscopy (HRTEM), energy dispersive (EDS), and electron energy-loss spectroscopy (EELS). Atom-probe tomography (APT) is a powerful technique to investigate phase transformations and diffusion at the sub-nanoscale as it has the unique capability to map atomic species in three dimensions, with 0.1 and 0.3 nm depth and lateral resolutions, respectively.[10–13] The technique is based on the combination of laser- and field-assisted evaporation of surface atoms; evaporated atoms are collected by a time-resolved and position-sensitive detector for chemically resolved 3D reconstruction, enabling the computation of interface profiles.

In polycrystalline thin-film structures, the effects of diffusion are determined by lattice (D_L) and grain boundary (D_{GB}) diffusion constants, according to the model of Harrison.[6] Dominant grain-boundary diffusion with $D_{GB} \gg D_L$, is the Harrison type C regime: grain boundaries short-circuit atomic diffusion. More comparable lattice and grain-boundary diffusivities, with $D_{GB} > D_L$, result in the Harrison type B regime, with diffusion first along grain boundaries and then into the center of grains. Finally, where grain-boundary and lattice diffusivities are roughly equal, $D_{GB} \approx D_L$, atoms diffuse both vertically through interfaces and laterally from the grain boundaries toward the inner parts of the grains. In previous work, APT resolved preferential grain-boundary diffusion in NiFe/Cu,[14] Cu/Co,[11] and Pt–Rh–Ru (Ref. 15) layers. In this study, we investigate diffusion in Cu/Co/IrMn/Pt exchange bias structures with

a)jean-marie.lebreton@univ-rouen.fr
b)vincent.baltz@cea.fr

various thicknesses of the Pt cap. APT images are correlated to the films' exchange bias properties at different steps of the diffusion, i.e., after various annealing conditions.

II. EXPERIMENTAL PROCEDURE

For this study, two Ta (3 nm)/[Cu (3 nm)/Co (3 nm)/IrMn (7 nm)]$_n$/Pt (t_{Pt}) multilayer structures were deposited by dc-magnetron sputtering with an Ar pressure of 2.5×10^{-3} mbar onto thermally oxidised silicon substrates, Si/SiO_2//. In the two multilayer structures, Co (3 nm) was the F layer and IrMn (7 nm) was the AF layer, made from an $Ir_{20}Mn_{80}$ target (at. %). The Ta (3 nm)/Cu (3 nm) bilayer was used as buffer and the top Pt film was the capping layer, preventing the stack from oxidation in air. The two structures differ in the thickness of the Pt, $t_{Pt} = 2$ and 80 nm. The substrate holder temperature was monitored during deposition and remains constant near 16 °C. Incoming atoms during deposition may temporarily raise the temperature of the surface layer before thermalization; this would not be resolved by the temperature of the substrate holder, given the relative volumes of the surface layers and of the thermal reservoir. The sputtering targets were powered between 50 and 100 W to minimize heating during deposition. Deposition rates for Ta, Cu, Co, IrMn and Pt are measured as 0.14, 0.22, 0.11, 0.17, and 0.26 nm/s, respectively.

For studies of EB, room temperature EB was set by post-deposition field cooling (FC) of the samples for 60 min in a resistive furnace from an initial temperature T_{init} down to room temperature, with $T_{init} = 250$, 400, 450, 500 °C. The vacuum level during annealing is set to 10^{-6} mbar.[16] Positive magnetic field during cooling is applied in the sample plane, with an amplitude of 2.5 kOe, large enough to saturate the Co layers. Following this initial FC, all the AF entities with a blocking temperature (T_B) larger than room temperature were oriented toward the positive direction.[16–19] Room temperature hysteresis loops were then measured along the FC direction by vibrating sample magnetometry (VSM).

Following this step, sharp needles for APT characterization were formed by standard Ga+ focused ion beam (FIB) etching. The needles were mounted on holders for laser-assisted APT experiments imaging atomic species Cu, Co, Ir, Mn, and Pt. Details of the FIB preparation and APT measurement can be found in Refs. 10, 20, and 21. Although the base structure of interest contains a single repetition (n = 1), multilayer stacks with n = 7 were used to ease the analysis of the APT measurements. Also in an attempt to ease the APT measurements, a thick cap layer was used to avoid deterioration of the top Cu/Co/IrMn layer during the FIB thinning process, given that only the Si/SiO_2//Ta (3 nm)/[Cu (3 nm)/Co (3 nm)/IrMn (7 nm)]$_7$/Pt (80 nm) samples with various T_{init} were measured by APT.[20] We will see further down that this will suit to interpret both cases: $t_{Pt} = 2$ and 80 nm. APT analyses were performed with a flexible tomographic atom probe (FlexTAP from CAMECA) at 80 K, using a 342 nm laser with 350 fs pulses and a 36° collection angle for optimal mass resolution. The analyses being made with a wide angle, which corresponds to a wide surface (typically $100 \times 100\,nm^2$), layer images appear deformed at the edges of the analysed volume. However, flat layers (and thus flat interfaces) were obtained on a $30 \times 30\,nm^2$ surface. Scaling of the APT data sets was performed by considering the Pt cap (111) planes that were systematically identified by field ion microscopy. This latter technique gives information on the crystallography of the sample under investigation.

III. RESULTS AND DISCUSSION

Figure 1 shows room temperature VSM hysteresis loops for the samples, field-cooled (FC) from various T_{init}, and with different cap thicknesses $t_{Pt} = 2$ and 80 nm. For both Pt cap thicknesses, for annealing above $T_{init} = 400$ °C, the exchange bias loop shift H_E reduces, the saturation magnetization M_S decreases, and the coercive squareness decreases. In addition, from Fig. 1, it is clear that the thermally activated modifications of H_E, M_S, and coercive squareness are reached at lower temperatures for the sample with the 80 nm Pt cap. We use the APT to find a microscopic basis for both the common and different features observed in the 2 and 80 nm Pt-capped films.

Figure 2 shows a 2D projection of the 3D reconstruction after APT analysis and Fig. 3 shows the corresponding concentration profiles. We focus our attention on a

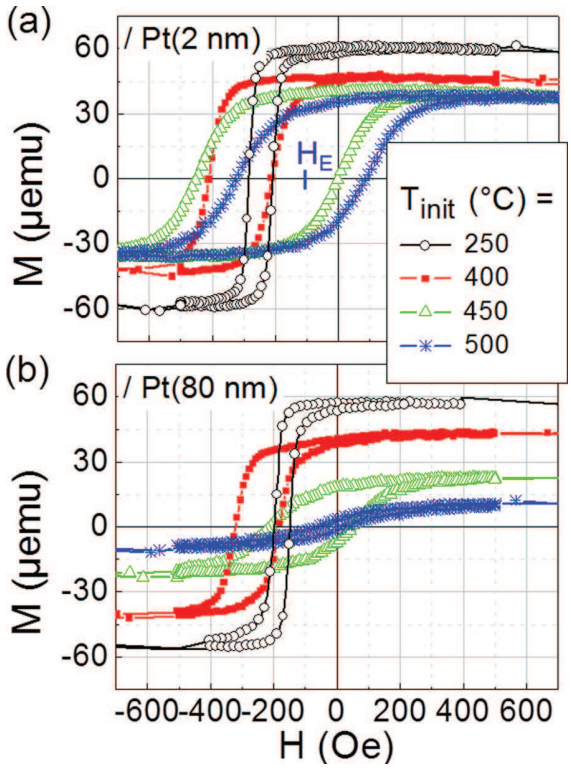

FIG. 1. Hysteresis loops measured at room temperature by VSM along the FC direction for samples with composition: Si/SiO_2//Ta (3 nm)/Cu (3 nm)/Co (3 nm)/IrMn (7 nm)/Pt (t_{Pt}) with a Pt thickness, t_{Pt} of (a) 2 and (b) 80 nm, and for various initial FC temperatures, T_{init}. The samples are FC from T_{init} for 60 min down to room temperature (~25 °C) with $T_{init} = 250$, 400, 450, 500 °C. The hysteresis loop shift, H_E for $T_{init} = 500$ °C and $t_{Pt} = 2$ nm is defined in (a).

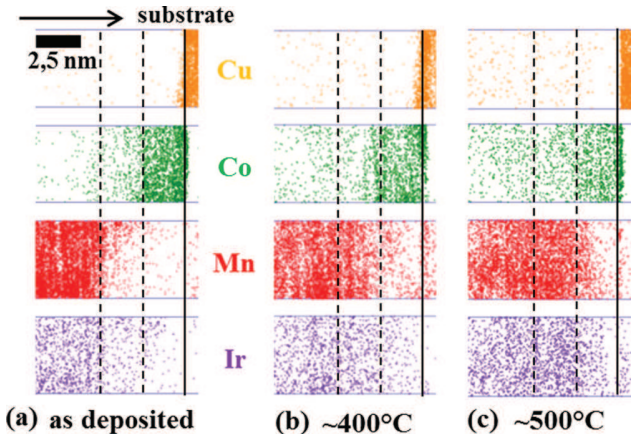

FIG. 2. Atom probe 2D projection of the 3D-reconstruction corresponding to the spatial distribution of Cu, Co, Mn, and Ir atoms in a /Cu (3 nm)/Co (3 nm)/IrMn (7 nm)/ sub-repetition: (a) as-deposited state and after annealing from T_{init} for 60 min down to room temperature with (b) $T_{init} \sim 400\,^{\circ}C$ and (c) $T_{init} \sim 500\,^{\circ}C$. For the sake of clarity, the atomic projections are plotted separately. The straight line indicates the sharp Cu/Co interface; the dashed indicates the diffused Co/IrMn interface. The scale marker in (a) is common to (a)–(c) and for the three images, the total depth is 9 nm. The image cross-section is $5 \times 5\,nm^2$.

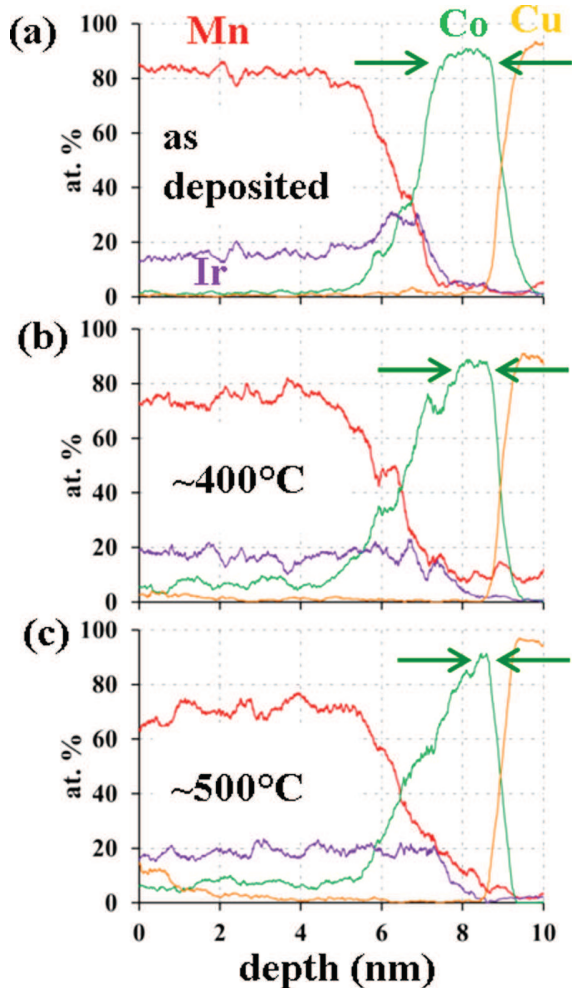

FIG. 3. Cu, Co, Mn, and Ir concentration profiles for /Cu (3 nm)/Co (3 nm)/IrMn (7 nm)/ sub-repetitions: (a) as deposited and after annealing from T_{init} for 60 min down to room temperature with (b) $T_{init} \sim 400\,^{\circ}C$ and (c) $T_{init} \sim 500\,^{\circ}C$. The error is estimated to be $\pm 1\%$. The cross-section of the region of interest investigated is $5 \times 5\,nm^2$.

/Cu (3 nm)/Co (3 nm)/IrMn (7 nm)/ sub-stack of the Si/SiO_2// Ta (3 nm)/$[Cu\ (3\,nm)/Co\ (3\,nm)/IrMn\ (7\,nm)]_7$/Pt (80 nm) sample. This sub-stack is the second of the seven repetitions from the cap and is typical of all the sub-stacks and interfaces except for the last IrMn (7 nm)/Pt (80 nm) interface, discussed further on. Figure 2(a) shows that the Co/IrMn interface is already diffused as deposited.[22] A sub-density at the Co/IrMn interface can be observed. This is an artefact due to the difference in the evaporation fields of the IrMn and Co layers (34 V/nm and 37 V/nm, respectively).[23] This effect is much less pronounced for the annealed samples, Figs. 2(b) and 2(c), because the transition from Co to IrMn is less abrupt compared to the as-deposited samples. Intermixing during the deposition process is ascribed in part to physical mechanisms (e.g., knock-on exchange) and in part to chemical mechanisms (e.g., negative bond enthalpy between elements). The incoming atoms during deposition may temporarily raise the temperature of the already-deposited surface layer before thermalization, as mentioned in Sec. II. From Figs. 2(b) and 2(c), we observe that further annealing the sample significantly increases Co and Mn intermixing. The intermixing is clearly visible in the concentration profiles plotted in Fig. 3: the width of the plateau in the Co profile progressively shrinks as the annealing temperature increases, as indicated by the arrows, and the concentration profile for both Co and Mn becomes less abrupt at the IrMn/Co interface. Thermally activated Co-Mn intermixing that increases with temperature very likely contributes to the observed degradation of magnetic properties common to both t_{Pt}. Note that both 3D reconstructions (Fig. 2) and concentration profiles (Fig. 3) show that the Cu/Co interface remains sharp, consistent with bulk immiscibility of Cu and Co at 400 and at 500 °C.[24] The apparent slight increase in Cu concentration in the IrMn layer at 500 °C likely originates in diffusion from upper layers of the $n = 7$ stack, and is not relevant for the primary repeat.

Next, we focus on the topmost IrMn (7 nm)/Pt (80 nm) interface. Figure 4 shows the 3D reconstruction and extracted 2D interface profile. The interface is sharp, with little Pt-Mn intermixing observed. In addition, note the well-defined atomic planes in the Pt layer. Note that (111) planes were identified by field ion microscopy, which gives information on the crystallography. We obtained the same results as in Ref. 20. In Fig. 5, the APT image taken after annealing at 400 °C shows that *within* a grain, the IrMn/Pt interface remains sharp. On the other hand, at Pt grain boundaries, APT reveals a high concentration of Mn, consistent with grain-boundary diffusion of Mn in Pt. The observed behaviour is consistent with the Harrison type-C regime of diffusion,[6] where grain boundaries and other planar defects offer paths with enhanced atomic mobility and $D_{GB} \gg D_L$. In these images, Mn mobility in Pt grain boundaries is shown to exceed 30 nm after annealing at 400 °C. A concentration profile obtained through a grain boundary [Fig. 5(d)] shows that the measured Mn concentration is about 7 at. % at the centre of the grain boundary. Considering the accuracy of the reconstruction procedure, and the size of the numerical sampling boxes used to obtain such a concentration profile,[25] this measured concentration

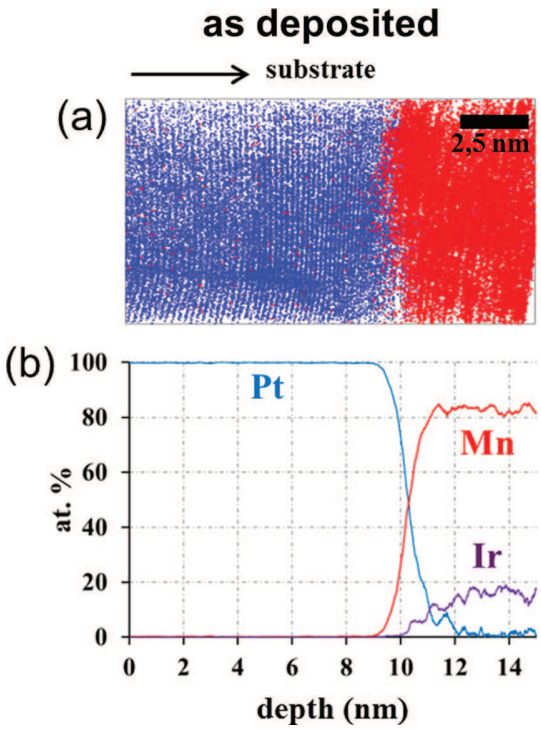

FIG. 4. (a) Atom probe reconstruction of Pt and Mn in the topmost /IrMn (7 nm)/Pt (80 nm) layers, as deposited, Ir excluded for clarity. (b) Corresponding concentration profiles, including Ir.

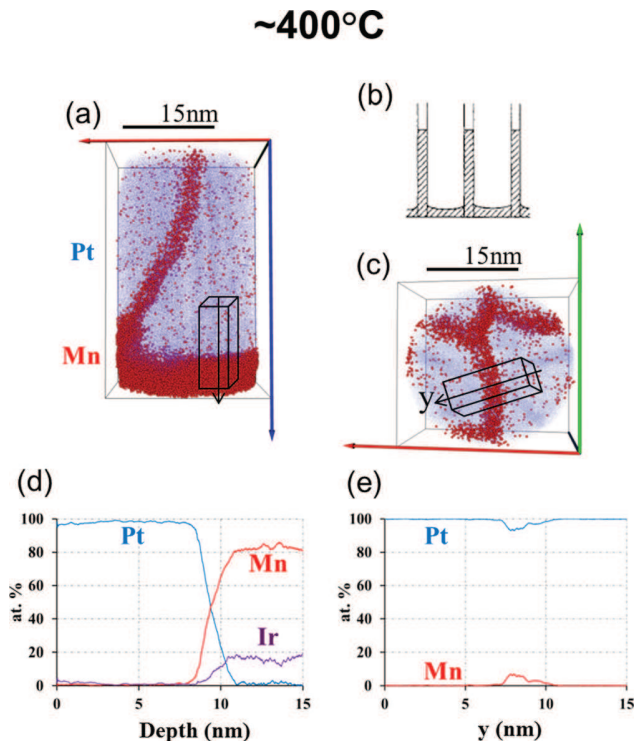

FIG. 5. (a) Pt and Mn in the topmost /IrMn (7 nm)/Pt (80 nm) layers after annealing from ~400 °C. (b) Illustration of Harrison type C diffusion[5,6] (grain-boundary-dominant). (c) Top view, same system as (a). (d) Pt, Mn, and Ir concentration profiles extracted from the window in (a). (e) Pt and Mn concentration profiles extracted from the window in (c).

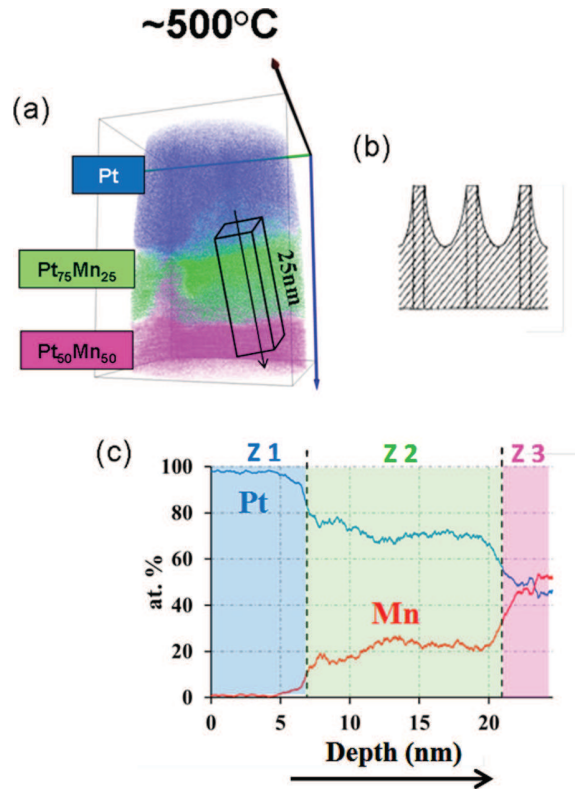

FIG. 6. (a) Pt and Mn in the topmost /IrMn (7 nm)/Pt (80 nm) layers after annealing to ~500 °C. The atomic compositions refer to the approximate stoichiometry within the grains in the middle of the various phases. (b) Corresponding side view sketch, after Ref. 5, of diffusion at interfaces and along the grain boundaries (Harrison type B behavior[6]). (c) Pt and Mn concentration profiles extracted from window plotted in (a). The color scheme in (c) is as follows: Pt for $x_{Pt} > 80$ at. %, $Pt_{75}Mn_{25}$ for 80 at. % $> x_{Pt} > 60$ at. %, and $Pt_{50}Mn_{50}$ for 60 at. % $> x_{Pt}$ with x_{Pt} the Pt atomic concentration.

corresponds to an estimated Mn concentration within the grain boundary of about 28 at. %.

The consequences of further annealing at 500 °C are shown in Fig. 6. Here, we observe Mn diffusion both across the IrMn/Pt interface within grains and along grain boundaries, typical of the Harrison type B regime [*ibid*]. The distribution of Pt and Mn atoms across the IrMn/Pt interface shows a gradual variation of concentrations, revealing different regions: pure Pt (Z1), $Pt_{75}Mn_{25}$ (Pt_3Mn, at. %) region (Z2), $Pt_{50}Mn_{50}$ (at. %) region (Z3). Mn diffusion from IrMn into Pt and the subsequent formation of well-known Pt-Mn phases[26] are in agreement with the larger affinity between Mn and Pt atoms than between Mn and Ir. In other words, the enthalpy of formation of Pt_3Mn and PtMn is certainly lower than that of IrMn. Therefore, Pt acts as a getter for Mn: the higher the annealing temperature, the more the Mn atoms become captured by the Pt layer and the more Mn-depleted the IrMn layer becomes. The observed behaviour is similar to oxygen-assisted diffusion for magnetic tunnel junctions when IrMn is close to an oxygen-based compound (AlO_x or MgO) with a lower enthalpy of formation than MnO_x.[8] We conclude that Pt-assisted diffusion of Mn may be important in these structures.

Finally, we consider the annealing-dependent magnetic measurements (Fig. 1) in light the temperature-dependent

diffusion, revealed by APT (Figs. 2–5). For both samples with different Pt layer thicknesses, Fig. 1 shows that the exchange bias loop shift H_E initially increases when T_{init} rises up to 400 °C. There are likely two sources for the initial increase in the EB field: first, resetting the exchange bias direction for grains with blocking temperature $T_B > 250$ °C;[17–19] second, interfacial diffusion, increasing the F-AF exchange coupling and reducing M_S. Above $T_{init} = 400$ °C, H_E reduces as the likely consequence of further thermally activated intermixing, pointed out by APT results revealing Mn diffusion at both Co/IrMn interfaces (>400 °C, Fig. 5) and IrMn/Pt interfaces (>500 °C, Fig. 6). Meanwhile, and for similar reasons, M_S decreases and the magnetizations' reversals become smoother and smoother. Concerning Mn diffusion on the Co/IrMn side, our findings agree with earlier Auger electron spectroscopy (AES), Rutherford backscattering spectroscopy (RBS), and VSM studies of Ta/NiFe/Cu/NiFe/IrMn/CoFe/X with X = natural oxidation and Ta.[9] Interestingly, Figure 1 also shows that for a given T_{init}, H_E is larger for $t_{Pt} = 2$ nm compared to $t_{Pt} = 80$ nm. One possibility is that the IrMn layer relaxes differently depending on the thickness of the Pt cap. However, we can understand this more rapid degradation of magnetic properties as the influence of a larger Pt reservoir for Mn diffusion out of the IrMn layer. We note that Pt has been used in the past to limit Co-IrMn interfacial mixing: once inserted between Co and IrMn, it traps the Mn atoms and forms a PtMn stable layer thus preventing Co and Mn mixing.[21] Since Pt is miscible with Co,[24] for the particular case of Co/IrMn bilayers, it was actually shown that inserting (Cu/Pt) dual barrier fulfils the manifold requirements of limiting Co-Mn, Co-Pt, and Cu-Mn intermixing which take place when using either no or single Pt and Cu barriers, respectively.[27]

IV. CONCLUSION

APT analysis of Cu/Co/IrMn/Pt multilayers, annealed at various temperatures, revealed Mn diffusion relevant for the optimization of exchange bias. On the IrMn/Pt side, APT clearly shows dominant Mn diffusion into Pt grain boundaries. The more rapid degradation of magnetic properties for the sample with a thick Pt cap is consistent with the role of Pt in gettering Mn from IrMn. The influence of the amount of Pt atoms in the topmost Pt cap turned out to be crucial. Alike oxidation-enhanced Mn diffusion for magnetic tunnel junctions with AlO_x and MgO, our observations may relate to platinum-assisted diffusion.

ACKNOWLEDGMENTS

W. E. Bailey of Columbia University, New York, is gratefully acknowledged for a critical reading of this manuscript.

[1]S. A. Wolf, D. D. Awschalom, R. A. Buhrman, J. M. Daughton, S. von Molna, M. L. Roukes, A. Y. Chtchelkanova, and D. M. Treger, Science **294**, 1488 (2001).
[2]J. Nogués and I. K. Schuller, J. Magn. Magn. Mater. **192**, 203 (1999).
[3]A. E. Berkowitz and K. Takano, J. Magn. Magn. Mater. **200**, 552 (1999).
[4]S. Yuasa and D. D. Djayaprawira, J. Phys. D: Appl. Phys. **40**, R337 (2007).
[5]M. Ohring, in *Materials Science of Thin Films*, 2nd ed. (Academic Press, San Diego, 2002), p. 641.
[6]L. Harrison, Trans. Faraday Soc. **57**, 1191 (1961).
[7]D. J. Larson, E. A. Marquis, P. M. Rice, T. J. Prosa, B. P. Geiser, S.-H. Yang, and S. S. P. Parkin, Scr. Mater. **64**, 673 (2011).
[8]C. S. Yoon, J. H. Lee, H. D. Jeong, C. K. Kim, J. H. Yuh, and R. Haasch, Appl. Phys. Lett. **80**, 3976 (2002).
[9]J. H. Lee, H. D. Jeong, C. S. Yoon, C. K. Kim, B. G. Park, and T. D. Lee, J. Appl. Phys. **91**, 1431 (2002).
[10]B. Gault, F. Vurpillot, A. Vella, M. Gilbert, A. Menand, D. Blavette, and B. Deconihout, Rev. Sci. Instrum. **77**, 043705 (2006).
[11]D. J. Larson, A. K. Petford-Long, Y. Q. Ma, and A. Cerezo, Acta Mater. **52**, 2847 (2004).
[12]A. Cerezo, P. H. Clifton, M. J. Galtrey, C. J. Humphreys, T. F. Kelly, D. J. Larson, S. Lozano-Perez, E. A. Marquis, R. A. Oliver, G. Sha, K. Thompson, M. Zandbergen, and R. L. Alvis, Mater. Today **10**, 36 (2007).
[13]T. F. Kelly and M. K. Miller, Rev. Sci. Instrum. **78**, 031101 (2007).
[14]C. B. Ene, G. Schmitz, R. Kirchheim, and A. Hütten, Acta Mater. **53**, 3383 (2005).
[15]T. Li, P. A. J. Bagot, E. A. Marquis, S. C. E. Tsang, and G. D. W. Smith, J. Phys. Chem. C **116**, 17633 (2012).
[16]V. Baltz, Appl. Phys. Lett. **102**, 062410 (2013).
[17]V. Baltz, B. Rodmacq, A. Zarefy, L. Lechevallier, and B. Dieny, Phys. Rev. B **81**, 052404 (2010).
[18]S. Soeya, T. Imagawa, S. Mitsuoka, and S. Narishige, J. Appl. Phys. **76**, 5356 (1994).
[19]E. Fulcomer and S. H. Charap, J. Appl. Phys. **43**, 4190 (1972).
[20]L. Lechevallier, A. Zarefy, R. Lardé, H. Chiron, J. M. Le Breton, V. Baltz, B. Rodmacq, and B. Dieny, Phys. Rev. B **79**, 174434 (2009).
[21]A. Zarefy, L. Lechevallier, R. Lardé, H. Chiron, J. M. Le Breton, V. Baltz, B. Rodmacq, and B. Dieny, J. Phys. D: Appl. Phys. **43**, 215004 (2010).
[22]F. Letellier, V. Baltz, L. Lechevallier, R. Lardé, J.-F. Jacquot, B. Rodmacq, J.-M. Le Breton, and B. Dieny, J. Phys. D: Appl. Phys. **45**, 275001 (2012).
[23]A. Zarefy, R. Lardé, L. Lechevallier, F. Cuvilly, J. M. Le Breton, V. Baltz, B. Rodmacq, and B. Dieny, J. Appl. Phys. **105**, 103912 (2009); A. Zarefy, Ph.D. thesis, University of Rouen, 2011.
[24]R. M. Bozorth, *Ferromagnetism* (D. Van Nostrand Company, Inc., 1951).
[25]R. Lardé, L. Lechevallier, A. Zarefy, A. Bostel, J. Juraszek, J. M. Le Breton, B. Rodmacq, and B. Dieny, J. Appl. Phys. **105**, 084307 (2009).
[26]L. Lechevallier, A. Zarefy, F. Letellier, R. Lardé, D. Blavette, J. M. Le Breton, V. Baltz, B. Rodmacq, and B. Dieny, J. Appl. Phys. **112**, 043904 (2012).
[27]K. Akmaldinov, S. Auffret, I. Joumard, B. Dieny, and V. Baltz, Appl. Phys. Lett. **103**, 042415 (2013).